Physics Letters A 381 (2017) 663–670

Contents lists available at ScienceDirect

Physics Letters A

www.elsevier.com/locate/pla

Metal mono-chalcogenides ZnX and CdX (X = S, Se and Te) monolayers: Chemical bond and optical interband transitions by first principles calculations

Mandana Safari [a], Zohreh Izadi [a], Jaafar Jalilian [a,*], Iftikhar Ahmad [b,c], Saeid Jalali-Asadabadi [d]

[a] Young Researchers and Elite Club, Kermanshah Branch, Islamic Azad University, Kermanshah, Iran
[b] Center for Computational Materials Science, University of Malakand, Chakdara, Pakistan
[c] Abbottabad University of Science & Technology, Abbottabad, Pakistan
[d] Department of Physics, Faculty of Science, University of Isfahan (UI), Hezar Gerib Avenue, Isfahan 81746-73441, Iran

ARTICLE INFO

Article history:
Received 25 August 2016
Received in revised form 26 November 2016
Accepted 29 November 2016
Available online 9 December 2016
Communicated by F. Porcelli

Keywords:
Metal mono-chalcogenide
Optical transition
Chemical bond
Energy band gap
Absorption spectrum

ABSTRACT

In this paper, we explore the structural, electronic and optical properties of ZnX and CdX (X = S, Se and Te) compounds in the two-dimensional (2D) graphene-like structure using the full potential augmented plane waves plus local orbitals (FP-APW + *lo*) method. Unlike their bulk phase, they are optically inactive because of their indirect band gap nature except CdS and ZnS. These two compounds maintain their direct band gap nature and hence are optically active. The static dielectric constants for these monolayers illustrate increasing trend with decrease in the band gap values. Furthermore, an acceptable description of electron transitions in these monolayers is accomplished according to the imaginary parts of the dielectric functions and absorption spectra in ZnS and CdS as examples of each group of CdX and ZnX. The results presented in this article revealed that ZnS and CdS in the 2D structure can be effectively used in optoelectronic devices such as solar cell materials and so forth.

1. Introduction

Metal mono-chalcogenides especially cadmium and zinc based groups II–VI compounds with general formula CdX and ZnX, where X represents S, Se and Te, are the commonly used chalcogenide materials with 1:1 stoichiometry [1,2]. They are known for their wide range of band gaps, from IR to UV, which make them suitable for many high-tech applications in our progressing world. These compounds have extensive applications in optical waveguides [3], photovoltaic devices [4], blue light emitting diodes [5–7], blue lasing materials [3], photo detectors [8], solar cells [9], along with catalyst applications [10]. Moreover, thin film transistors, THz emitters, detectors and imaging systems would not have existed without these chalcogenides [11]. These wide range of applications in the optoelectronic industry makes them ideal compounds for theoretical and experimental studies.

In the bulk form, the cadmium and zinc based groups II–VI semiconductors crystallize in two main phases, zincblende and wurtzite [12]. The first-ever monolayer of CdSe was reported by Lister and Stickney [13] in 1996 using the electrochemical atomic layer epitaxy (ECALE) technique; however, they found it in wurtzite phase. After that, many others have tried to work on the synthesizing of these compounds too; e.g., S. Ithurra and B. Dubertret [14] synthesized quasi two dimensional (2D) colloidal CdSe platelets with the atomic level thicknesses. Gao and Wang [15] synthesized 2D single crystal CdS nanosheets; Mahdi et al. [16] also synthesized these compounds using the pulsed laser deposition technique. Although extensive theoretical studies are reported on the bulk and nanostructures of CdX and ZnX (X = S, Se and Te) to understand their structural, electronic and optical properties [12, 17,18], limited theoretical studies are available in the literature about the 2D graphene-like structure of these compounds. In 2012, the electronic and magnetic properties of the semi fluorinated CdS sheets were studied by Xiao et al. [19] using the PBE version of the generalized gradient approximation (PBE-GGA). Recently, Tang et al. [20] calculated the magnetic properties of carbon substituted CdS monolayer using the *ab initio* DFT calculations within GGA functional. Also Zheng et al. investigated II–IV semiconductor groups with LDA functional that the obtained results from this functional causes to an underestimation of energy gap values [21]. The physical properties of the compounds can be greatly influ-

* Corresponding author.
E-mail address: jaafarjalilian@gmail.com (J. Jalilian).

http://dx.doi.org/10.1016/j.physleta.2016.11.040
0375-9601/

Table 1
Calculated lattice parameters (in Å) and the cohesive energy (eV) for the 2D graphene-like structures are compared with the other available results.

	CdS	CdSe	CdTe	ZnS	ZnSe	ZnTe
Lattice parameter (Å)						
This work	4.24	4.44	4.76	3.88	4.10	4.43
Others	4.17[a]	4.45[b]	...	3.89[c]	...	...
Cohesive energy (eV)						
This work	−7.0	−5.97	−4.9	−6.12	−5.04	−44.22
Ref. [21]	−5.85	−5.31	−4.74	−6.68	−5.95	−5.17

[a] Ref. [32]; [b] Ref. [33]; [c] Ref. [34].

enced by quantum confinement effects in nanoscale structures. In this article, various physical properties of the CdX and ZnX (X = S, Se and Te), the flat form of honeycomb monolayers that could be created as a result of substrate effects, stress and strain condition and so forth, are explored using the density functional theory (DFT) approach to reveal the quantum confinement effects on these compounds. An unusual change from optically active nature to inactive form is observed for the compounds under study except CdS and ZnS, which have not been reported earlier. In order to obtain logical and rational results for these compounds, the calculations are carried out with one of the most recent and effective theoretical tools, mBJ-GGA [22]. This technique has proved its worth in our earlier studies on bulk samples of II-VI semiconductors [23–27]; therefore, it is expected to be also effective for these 2D structures of the II–VI semiconductors.

In this article in addition to identifying the bonding orbitals of atoms, we have explained the possible reasons for the variation of the direction of band gap by changing material phase from bulk to 2D state simultaneously. Optical investigation consists of finding the exact electron transitions in CdS and ZnS as active materials based on selection rules in hybridized orbital. These kinds of orbitals and their bond formation details can be found in the electronic part of this article. These data can help us to suggest their suitable applications and let them find their way even in solar cell devices and photocatalyst materials.

2. Computational details

In this theoretical work, the set of Kohn–Sham equations for 2D ZnX and CdX (X = S, Se and Te) compounds in graphene-like structure have been solved using the full potential augment plane waves plus local orbitals method (FP-APW + lo) within the framework of the DFT [28,29] implemented in the WIEN2k code [30]. The selection of appropriate exchange-correlation functional is of key importance in the DFT calculations. Therefore, to achieve the best results from our calculations, we use the modified Becke and Johnson exchange potential proposed by Tran and Blaha [22] and the generalized gradient approximation functional parameterized by Perdew–Burke–Ernzerhof (GGA-PBE) [31]. The cutoff parameter $R_{MT}K_{max}$ is set to "7", where R_{MT} is the smallest radius of the muffin-tin sphere radii and K_{max} denotes the largest k-vector to expand plane waves in the interstitial area. The G_{max} which determines the number of terms of the Fourier expansion of the charge density function in calculations is optimized to 14 $Ry^{1/2}$. Using the random phase approximation [32] (RPA), the dielectric tensors are derived to achieve the imaginary part of the dielectric function and the Kramers–Kronig relations are set out to achieve the real part of this function. Because of the need of heavy mesh for the optical calculation part, the $12 \times 12 \times 3$ and $30 \times 30 \times 7$ k-points mesh in the first Brillouin zone (1BZ) are considered to calculate the electronic and optical properties. Lorentzian broadening is considered with gamma equal to 0.1 eV. The volume optimization is necessary to achieve an unstrained monolayer for each compound in our study. Thus, we have employed Birch-Murnaghan equation of state [33] to get a more stable monolayer of each compound in an unstrained mode. The results of the relaxed lattice parameters are summarized in Table 1 and compared with other results [34–36].

Table 2
The comparison of our calculated energy band gaps (in eV) within PBE-GGA and mBJ-GGA functionals for the 6 compounds under question in the zinc blende structure with the other theoretical and experimental results.

	LDA	mBJ-LDA	GGA-PBE*	mBJ-GGA*	Exp.
CdS	1.37[a]	2.66[b]	1.159	2.69	2.55[c,d]
CdSe	0.76[a]	1.89[b]	0.630	2.015	1.90[c], 1.82[d]
CdTe	0.80[a]	1.56[b]	0.758	1.805	1.6[c,d], 2.55[c]
ZnS	2.37[a]	3.66[b]	2.086	3.657	3.78[c], 3.85[c], 3.82[d]
ZnSe	1.45[a]	2.67[b]	1.276	2.772	2.82[c,d], 3.24[c]
ZnTe	1.33[a]	2.22[b]	1.27	2.42	2.39[c,d], 3.36[c]

* Our results; [a] Ref. [12]; [b] Ref. [17]; [c] Ref. [36]; [d] Ref. [37].

Table 3
The comparison of our calculated energy band gaps (in eV) within PBE-GGA and mBJ-GGA functionals for the 6 compounds under question in the wurtzite structure with the other theoretical and experimental results.

	LDA	mBJ-LDA	GGA-PBE*	mBJ-GGA*	Exp.
CdS	1.36[a]	2.66[b]	1.176	2.743	2.58[c], 2.60[c]
CdSe	0.75[a]	...	0.662	2.075	1.83[c], 2.26[c]
CdTe	0.85[a]	...	0.837	1.861	1.60[c]
ZnS	2.45[a]	3.66[b]	2.173	3.776	3.91[c], 3.94[c]
ZnSe	1.43[a]	...	1.405	2.892	2.87[c]
ZnTe	1.48[a]	...	1.442	2.437	...

* Our results; [a] Ref. [12]; [b] Ref. [20]; [c] Ref. [36].

3. Results and discussions

3.1. Electronic properties

The II–VI semiconductors family, especially CdS, CdSe, CdTe, ZnS, ZnSe, and ZnTe as the well-known direct band gap materials, can be crystallized normally in the zinc blende and wurtzite structures in bulk [37].

As we mentioned, the flat honeycomb structure is our choice in this study. First of all, we must identify the structural stability of these structures by calculating the cohesive energy of each compounds. The cohesive energy can be calculated by this formula:

$$E_{binding} = E_{CdX(ZnX)} - E_{Cd(Zn)} - E_X, \quad (1)$$

where $E_{CdX(ZnX)}$, $E_{Cd(Zn)}$ and E_X are total energy of monolayers, isolated Cd or Zn atoms and isolated X atoms, respectively. The X represents for S, Se and Te. The results of these calculations are inserted in Table 1. With comparison between these values and the mentioned values in Ref. [21], the structural stability of these structures can be proved.

The existence of wide energy band gap is a significant characteristic which is of particular importance for determining their applications. The calculated band gap energies using the mBJ-GGA approach for the bulk samples of the compounds under study are compared with the other theoretical approaches and experimental techniques [38,39] in Tables 2 and 3.

As it can be seen from Tables 2 and 3, the mBJ-GGA results of this work are in good agreement with the experimental values in previous the researches. These results also provide direct band gaps for these chalcogenides (see supplementary data). It is worthy to mention here that mBJ-GGA is a reliable theoretical tool for these compounds. Hence, this approach may also be effective for the treatment of the low dimensional nanostructures of these compounds; therefore, in this study, we proceed with mBJ-GGA for the 2D structure of these compounds. Quantum confinement

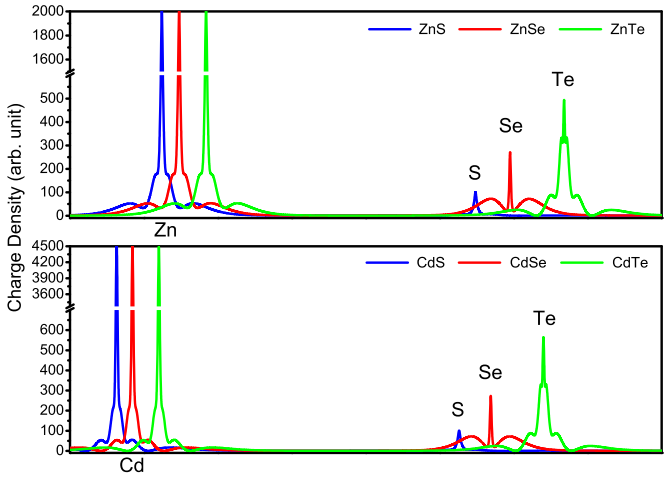

Fig. 1. The linear on-site charge distributions of ZnS (red), ZnSe (blue), ZnTe (green) in top panel, and of CdS (red), CdSe (blue) and CdTe (green) compounds in bottom panel. (For interpretation of the references to color in this figure legend, the reader is referred to the web version of this article.)

exerted on a compound in different low dimensional nanostructures such as graphene [40] and hexagonal BN [41] envisions the advent of new and perhaps useful features in physical and chemical properties of materials and nanostructures. So in this paper, we have compared the graphene-like nanosheet of these structures and have investigated their characteristics. Due to the higher level of accuracy that is obtained with mBJ functional compared with the other exchange-correlation approximations, we decided to use this functional to investigate the graphene-like structures of them. First of all, we focus on the linear on-site charge distribution in Fig. 1.

This figure obviously exhibits the different on-site charge distributions in these six compounds and can be a good criterion for the evaluation of ionic bond nature. It is obvious that the variation of on-site charge distribution of chalcogen atoms demonstrates the bonding nature move towards the ionic bond from the covalent bond with increasing anion radius, i.e. from sulfur to tellurium. This movement is obvious from observing the widening distribution of the electron density along the bonds in the counter plot of Fig. 2.

The shielding effect of internal electrons increases by increasing the atomic number which can lead to the less effect of nucleus attraction force on valence electrons. Furthermore, with respect to the electronegativity of anions (S = 2.58, Se = 2.55, Te = 2.10) and cations (Zn = 1.65, Cd = 1.69), the bonding nature movement from ionic toward covalent can be an understandable subject [42].

In order to achieve a better discussion on the electronic properties of these nanostructures, the total densities of states are presented in Fig. 3.

As it can be seen from total DOSs, the energy gaps for ZnX group are correspondingly larger than those of CdX group; the value of their energy band gaps is given in Table 4.

The energy band gaps of these compounds change depending on the type of the chalcogen atoms that have contributed in bond, so that a significant reduction in band gap value can be recognized for both branches as a companion consequence of atomic number and anionic radius increasing from sulfur to tellurium atoms. We turn to the study of the hybridization and the bonding mechanisms of these materials here. Since the behavior of CdX and ZnX branches in total DOS is similar to each other, we have concentrated on ZnS and CdS partial DOS as examples of each branch (see Fig. 4).

With due attention to the structural symmetries on one hand and s orbital overlapping with p orbital on the other hand, as it is clear from Fig. 4c and 4d, one can conclude that sp^2 hybridized orbitals are formed. Broadening of these two orbitals (s and p) in the same range of energy confirms this fact. In fact, $sp^2 - p$ bonding orbital is the total orbital that shows the overlapping of sp^2 hybridized orbital of S and Cd(Zn) atoms with p_z orbital of sulfur atoms in this flat form of graphene-like structures.

The corresponding antibonding orbitals allocates the conduction band naturally. In Fig. 4a and 4b, one can see a distinguished peak in −1 eV to 0 eV range that denotes to that part of p orbital in sulfur atoms directed perpendicular to the monolayer plane (z direction); this orbital is fully occupied and remains below the Fermi level, as it can be observed obviously in Fig. 4a and 4b compared to Fig. 4e and 4f. With regards to the energy level of p_z orbital locating around the Fermi level, this orbital plays a crucial role in the properties of these nanostructures. Some of its roles will be studied in the optical session. $sp^2 - p$ antibonding orbitals allocate such energy levels that have located above the Fermi level, so they form the edge of conduction band minimum (CBM). These orbitals are extended in sort of wide range of energy as well. They can

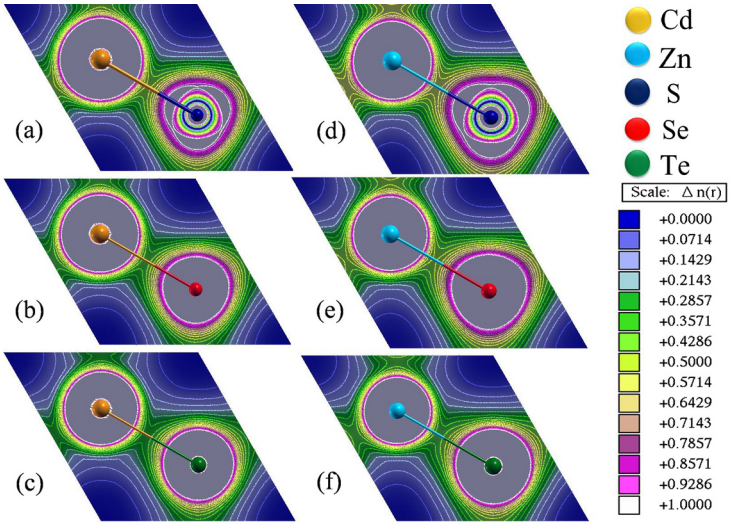

Fig. 2. Two dimensional charge density of (a) CdS, (b) CdSe, (c) CdTe, (d) ZnS, (e) ZnSe and (f) ZnTe compounds. Magnitude of the charge density is expressed by colors, with the blue at one end of the spectrum being the smallest and the white at the other end the largest. (For interpretation of the references to color in this figure legend, the reader is referred to the web version of this article.)

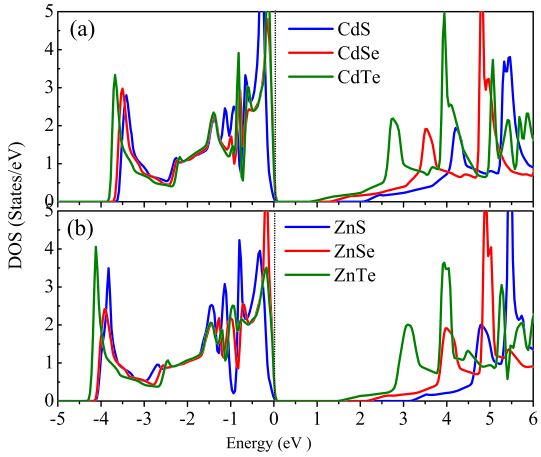

Fig. 3. Calculated total DOSs for all compounds.

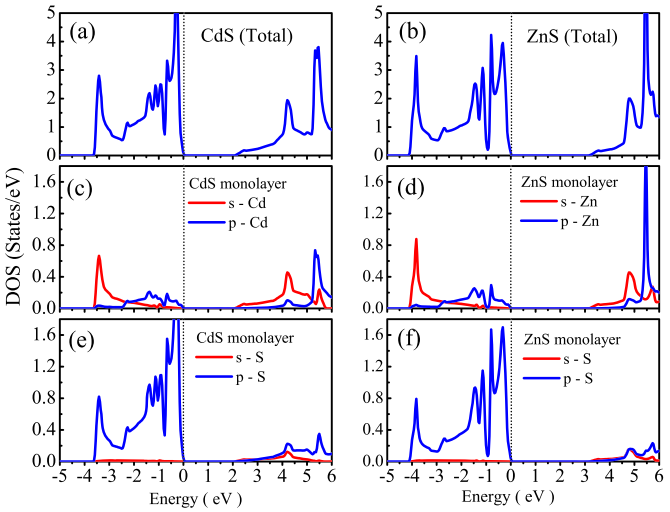

Fig. 4. Calculated total DOSs for (a) CdS, and (b) ZnS, as well as partial DOSs for s and p orbitals of (c) cadmium for CdS monolayer, (d) zinc for ZnS monolayer, (e) sulfur for CdS monolayer, and (f) sulfur for ZnS monolayer.

Table 4
The calculated energy gap in eV by mBJ-GGA and PBE-GGA functional for all monolayers.

	ZnS	ZnSe	ZnTe	CdS	CdSe	CdTe
mBJ-GGA	3.2	2.15	1.5	2.1	1.3	0.86
PBE-GGA	2.47	1.57	1.12	1.55	0.91	0.59

be the destination of the first electrons after excitation. In 5 eV to 6 eV range of energy, the p_z orbital of cadmium (zinc) atoms show up with a significant peak. This orbital in cadmium (zinc) atom is completely unoccupied and is located in the perpendicular direction to (x, y)-plane, which can also involve in a weak interaction with p_z orbital of sulfur atom. This interaction occurs as a partial charge exchange between these two orbitals. The electron density of these structures illustrates in perpendicular to nanosheet plane and shows this partial charge exchange (see Fig. 5).

The energy band gaps of these structures in bulk phase were reported as direct band gaps [8,12], and data have been reported here is in good agreement with these previous works (see supplementary data). The monolayer energy band structures of these compounds will be investigated below.

Band structures of these compounds in honeycomb structures in −1 eV to 5 eV range of energy are shown in Fig. 6.

Although the CdS and ZnS band structures indicate the direct band gaps, CdSe, CdTe, ZnSe and ZnTe are of indirect band gaps clearly. Here, two descriptions have been presented for more explanation about the difference of energy gap direction in CdS and ZnS monolayers in comparison with CdSe, CdTe, ZnSe and ZnTe monolayers:

1. Regarding electronic arrangement of chalcogen atoms (S: [He] $3s^2 3p^4$; Se: [Ne] $4s^2 4p^4$; Te: [Ar] $5s^2 5p^4$), one can find out their valence orbitals which have different energy levels in comparison with each other. Also p orbital energetically located farther from s orbital in the valence shell by increasing atomic number (the difference between energy levels of s and p orbitals in the valence shell becomes larger by increasing atomic number). The hybridized orbitals have been situated in lower energy levels compared with the participated orbitals before bond formation. This trend gets intense with an in-

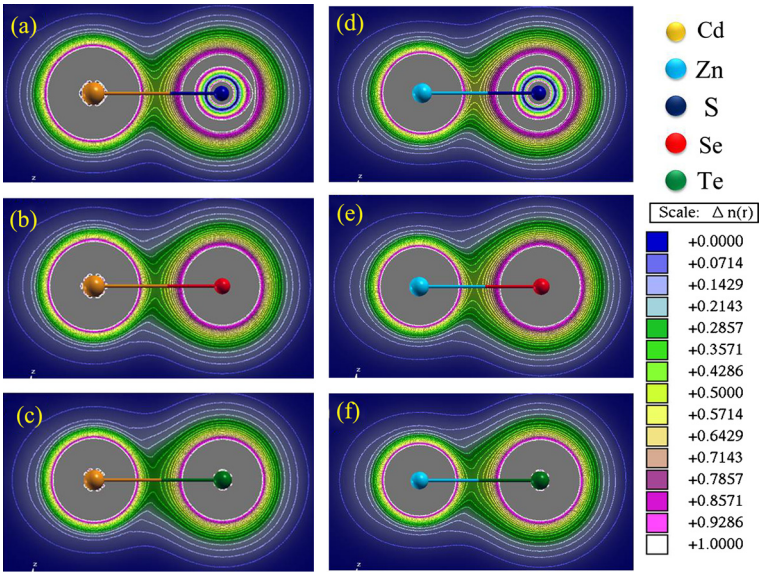

Fig. 5. 2D charge density distribution of (a) CdS, (b) CdSe, (c) CdTe, (d) ZnS, (e) ZnSe and (f) ZnTe compounds, colors are representation for magnitude of the charge density distribution, with blue at one end of the spectrum as the smallest value and white at the other end as the largest one. (For interpretation of the references to color in this figure legend, the reader is referred to the web version of this article.)

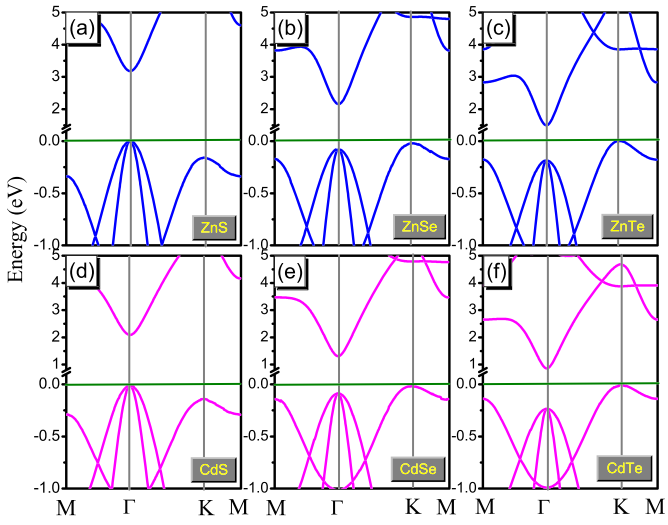

Fig. 6. Band structures for all compounds by mBJ-GGA functional. The band gaps have varied in two types of direct and indirect bands in CdSe, CdTe, ZnSe and ZnTe; however, it have remained direct for CdS and ZnS.

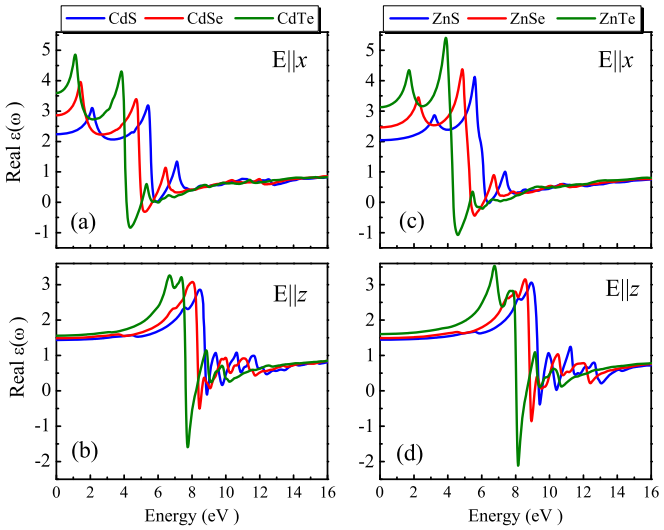

Fig. 7. The real parts of dielectric function have been plotted for x and z direction; (a) CdS (blue), CdSe (red), CdTe (green) for $E||x$; (b) CdS, CdSe, CdTe for $E||z$; (c) ZnS (blue), ZnSe (red), ZnTe (green) for $E||x$; (d) ZnS, ZnSe, ZnTe for $E||z$. (For interpretation of the references to color in this figure legend, the reader is referred to the web version of this article.)

crease in the atom's radius, so bond formation in CdTe (ZnTe) and CdSe (ZnSe) makes bonding orbitals in a lower level than that in CdS (ZnS).

2. On the other hand, the p_z orbitals of chalcogen atoms and Cd(Zn) atoms have interactions with each other (see Fig. 5). Once atomic number increases, the interaction between the nearest p_z orbitals becomes further. These interactions lead to an increase in the amount of energy of p_z orbital to higher amount of energy in CdSe, CdTe, ZnSe and ZnTe than that in CdS and ZnS.

Both of these phenomena have resulted in indirect band gaps in CdSe, CdTe, ZnSe and ZnTe. It is known that the direct band gap makes a material optically active, while an optically inactive material is characterized by its indirect band gap because of involving phonon in electron transition [24]. Therefore, these graphs imply that CdS and ZnS maintain their active mode when they are 2D nanosheets, but the optical nature of CdSe, CdTe, ZnSe, and ZnTe changes to inactive mode compared to the nature of bulk samples.

3.2. Optical properties

As mentioned earlier, CdS and ZnS maintain their optically active nature in the graphene-like monolayers; therefore, the knowledge of the optical properties of these monolayers is important for their applications in various optoelectronic devices. The optical properties of a material are related to the complex dielectric function, so in order to understand the optical properties of these compounds it is necessary to discuss the complex dielectric function for these compounds and then relate it to the absorption mechanism.

Complex dielectric function explains the linear behavior of a system subjected to the electromagnetic radiation. Thus, the understanding of this function is a key factor to know the optical properties of a material. As it is shown below, the complex dielectric function consists of two parts: the real and imaginary parts,

$$\varepsilon_{complex} = \Re\big[\varepsilon(\omega)\big] + i\Im\big[\varepsilon(\omega)\big] \ . \tag{2}$$

The real part of this function describes polarization and the imaginary part deals with the absorption of a material. The imaginary part is calculated using the following equation which is based on the random phase approximation (RPA) method:

$$\Im\big[\varepsilon_{\alpha\alpha}(\omega)\big] = \frac{4\pi^2 e^2}{m^2\omega^2}\sum_{i,f}\int \frac{2dk^3}{(2\pi)^3}\big|\langle ik|p_\alpha|fk\rangle\big|^2 \times f_i^k(1-f_f^k)\delta(E_f^k - E_i^k - \omega) \ . \tag{3}$$

This equation represents the contribution of interband transition [43], where $|ik\rangle$ represents the state vector for initial position and $|fk\rangle$ represents the state vector for the final position. f_i^k and f_f^k represent Fermi distribution function of occupied and unoccupied states, respectively. The real part of the complex dielectric function is calculated using the imaginary part in the Kramers–Kronig relations as below:

$$\Re\big[\varepsilon_{\alpha\beta}(\omega)\big] = \delta_{\alpha\beta} + \frac{2}{\pi}\,\mathrm{Pr}\int_0^\infty \frac{\omega'\Im\big[\varepsilon_{\alpha\beta}(\omega')\big]}{\omega'^2-\omega^2}d\omega' \ , \tag{4}$$

where Pr denotes the Cauchy principle part of the integral [44]. This equation is used to calculate the real part of the complex dielectric function for all the monolayers under study, for both directions of electric field polarizations, i.e. parallel to the monolayer plane ($E||x$) and perpendicular to the plane ($E||z$). It is clear from the plots (Fig. 7) that the static dielectric constant, which is known as dielectric constant of matter in the presence of static electric fields ($\Re\big[\varepsilon(\omega=0)\big]$) [45], increases with the decrease in band gap energy for both directions of polarization.

The calculated values for these constants are provided in Table 5. The relationship between band gap energy and static dielectric constant has been reported [46], and the present study follows that trend.

The plots and data also reveal that the variation of these values for perpendicular component of $E(E||z)$ is less remarkable than the parallel component. Furthermore, the behavior of the real dielectric function for high frequency (function's value for $\omega\to\infty$) demonstrates converging point for all graphs ($\Re\big[\varepsilon(\omega\to\infty)\big]=1$); this

Table 5
Static dielectric constant for both directions of E polarization calculated in this work.

Directions	ZnS	ZnSe	ZnTe	CdS	CdSe	CdTe
$E||x$	2.04	2.46	3.12	2.23	2.86	3.59
$E||z$	1.44	1.49	1.60	1.43	1.48	1.55

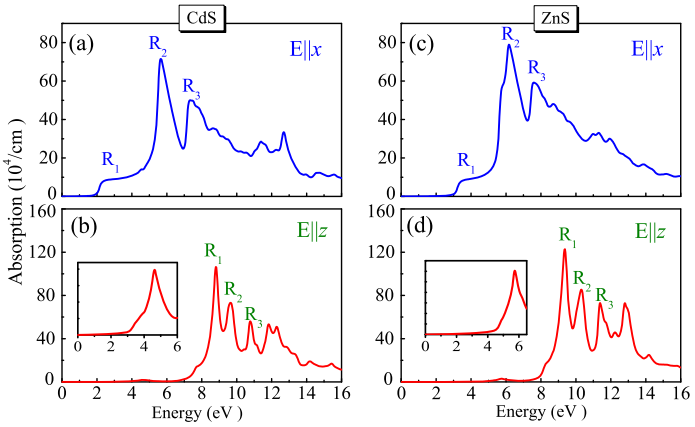

Fig. 8. Optical absorption spectrum: (a) CdS for $E||x$; (b) CdS for $E||z$; (c) ZnS $E||x$; (d) ZnS $E||z$; R_1, R_2 and R_3 refer to main peak of CdS and ZnS compounds for investigating interband transitions; the first absorption threshold are shown as inserted pictures in z direction.

Table 6
Threshold of photon absorption compared with electromagnetic spectrum.

Infrared spectrum (124 meV–1.7 eV)	CdSe, CdTe, ZnTe
Visible spectrum (1.7 eV–3.1 eV)	CdS, ZnSe
Ultraviolet spectrum (3.1 eV–124 eV)	ZnS

upper border is called optical dielectric constant. With the change in anion atom, no significant change is observed in this value, i.e. from sulfur to tellurium. On the other hand, the abnormal region of propagation [46] is shifted towards lower energy with the increase in the radii of anions, i.e. from sulfur to tellurium.

The imaginary part of dielectric function is directly related to the photon absorption in a compound. Our main concern is the study of the identified optically active ZnS and CdS monolayers; therefore, the absorption coefficient for these compounds are calculated using the imaginary part of the dielectric function in the following equation:

$$\alpha_{ij}(\omega) = \frac{\Im\left[\varepsilon_{ij}(\omega)\right]}{c n_{ij}(\omega)} \quad . \tag{5}$$

Here, $\Im\left[\varepsilon_{ij}(\omega)\right]$, $n_{ij}(\omega)$ and c are the imaginary part of the dielectric function, refractive index and the light velocity [47], respectively. The calculated absorption spectrum of ZnS and CdS is presented in Fig. 8.

It is clear from the plots that in the x direction, the first significant photon absorption occurs corresponding to the band gap values. This absorption generally relates to a particular region of the electromagnetic spectrum which can lead to specific applications of a compound in optoelectronic and photonic devices.

In semiconductors, the main absorption comes from interband transitions; therefore, we have determined three important regions for absorption by R_1, R_2 and R_3 labels corresponding to the interband transitions of CdS and ZnS (see Fig. 8). These three significant regions of absorption illustrate the increase in photon absorption for corresponding energy. The clear vision of the absorption mechanism for these compounds can be achieved by identifying the energy levels of the band structure engaged in every electron transition. The energy levels that may be useful in the description of electron transition in both compounds versus the Brillouin zone directions are presented in Fig. 9.

In the x direction, the first significant photon absorption occurs corresponding to the band gap values. The first rising compared with regions of the electromagnetic spectrum is identified in Table 6.

It is worth noting that the first absorption of photon for perpendicular polarization to monolayer plane has occurred in the high energy range of photons.

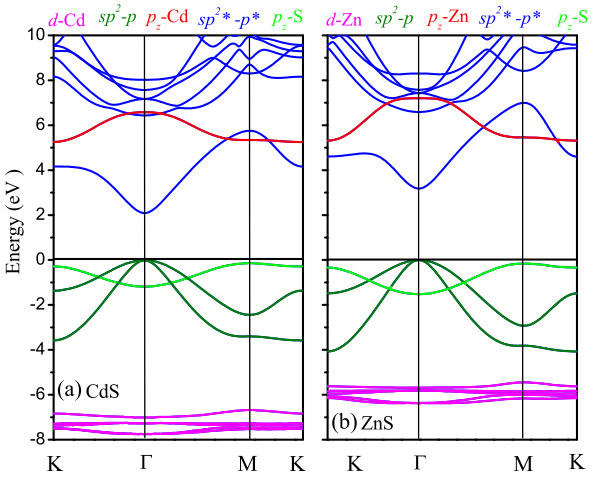

Fig. 9. Band structures for CdS and ZnS monolayers calculated by mBJ-GGA functional.

In details, the first region of the absorption spectrum for x direction belongs to adsorbed photons in the range 2.1–4.6 eV for CdS and 3.2–5.6 eV for ZnS. A photon absorbed in these ranges of energy can result in electron excitation from $3p_z$ orbital of sulfur atoms to $sp^2 - p$ antibonding orbitals. This transition occurs in that part of $sp^2 - p$ antibonding orbital which is of space symmetry of s^* in Cd atom (s antibonding orbital). On the other hand, the transition of excited electrons from $sp^2 - p$ orbitals to their corresponding antibonding orbitals also can contribute to the creation of this part of the absorption spectrum.

The second region of these spectra happens in the range 4.6–6.7 eV for CdS and 5.6–7.5 eV for ZnS, where the most percentage of the radiations is absorbed by the materials in this region. The absorption in this region consists of two kinds of electron transition. In the first portion, absorption happens due to the electron excitation in $sp^2 - p$ orbitals that choose corresponding antibonding orbitals as a destination, while another main portion in this region occurs when the unoccupied p_z orbital of Cd hosts excited electron from the occupied p_z orbital of S atom in CdS. In this compound, these electrons can transit to $sp^2 - p$ antibonding orbitals (with the preferable space symmetry of s orbital) and absorb photons in the range 5.44–5.6 eV. However, in ZnS monolayer, this kind of transition occurs in the range 5.6–6.4 eV.

The third region of absorption occurs when the electrons from the p_z orbital is hosted by $sp^2 - p$ antibonding orbitals; these electrons choose almost that part of the hybridized orbitals in which the space symmetry is close to p orbital symmetry.

As a consequence of the electric field of incident photons with out-of-plane polarization ($E||z$), electron transition obeys different patterns of initial and final orbitals with respect to the selection rules compared with transitions created by the parallel direction of the electric field ($E||x$).

The "R_1" labeled region of absorption in this direction of polarization belongs to 7.44–8.83 eV range of energy for CdS monolayer and 8.12–9.6 eV for ZnS monolayer. The most amount of absorption in this region is due to the electron transition from $sp^2 - p$ bonding orbitals to p_z orbital of Cd atom. These electrons in CdS monolayer may be hosted by $sp^2 - p$ antibonding orbitals (preferably s orbital space symmetry) under the condition of absorbing photons with specific energy of 8.7 eV. It is necessary to mention that these kinds of electrons in ZnS monolayer absorb photons in the range of 9.36–8.85 eV to transit between these two specific sites of energy.

The second region in absorption graphs (labeled as "R_2") in this direction ($E||z$) rises because of the increase in photon absorption by the electrons in p_z orbital of sulfur to move to $sp^2 - p$ antibonding orbitals, where the space symmetry of the hosted orbital has p symmetry. The third region (labeled as R_3) in these spectra is due to the transition of electrons from $sp^2 - p$ bonding orbital to $sp^2 - p$ antibonding orbitals with almost p space symmetry.

It is necessary to mention here that thresholds are always important from the application point of view, so we discuss them for the polarization of $E||z$. It can be seen from the figures (Fig. 8) that thresholds occur in lower energy with small peaks (these peaks are exaggerated by an inserted picture in Fig. 8 to give a better vision). It is illustrated in the plots that this region for CdS monolayer is in the range 4.0–5.57 eV, while it occurs in the range 5.0–6.0 eV for ZnS monolayer. These electrons are excited from $sp^2 - p$ bonding orbitals and p_z occupied orbital of sulfur to $sp^2 - p$ antibonding orbitals. It would be better to note here that these excited electrons choose that part of the hybridized orbitals as their destination which have space symmetry of s orbital; therefore, their final target is closer to $5s^*$ orbital (s antibonding orbital) in cadmium.

4. Conclusion

In summary, electronic and optical properties, along with the chemical bonding mechanism of the CdS, CdSe, CdTe, ZnS, ZnSe and ZnTe 2D graphene-like structures are investigated using the DFT approach with mBJ-GGA method. Some major results are listed here:

- The variation of on-site charge distribution of chalcogen atoms (in agreement with the electron density distribution and values of the electronegativity of anions and cations) demonstrates the bonding nature moves from covalent bond to ionic bond with increasing in anion radius, i.e. from sulfur to tellurium.
- The energy gap for ZnX group monolayers are correspondingly larger than those of CdX group, and the bond formation mechanism is investigated, which shows that the atoms of the monolayers bond through $sp^2 - p$ hybridization orbitals.
- The type of band gap is interestingly affected by bond formation mechanism such as the different energy values of bonding orbitals in different compounds and the weak interaction between p_z orbitals of adjacent atoms. It is concluded that the band gap nature of CdSe, CdTe, ZnSe and ZnTe transforms from direct to indirect.
- The optically active nature of all compounds in bulk phase changes into optically inactive nature in monolayer phase apart from CdS and ZnS. It is observed that the quantum confinement effects lead to the electronic rearrangement obviously in their bonding nature and orbital hybridization.
- Furthermore, the optical properties of the compounds are described by the complex dielectric functions. Their optical spectra get a red shift with increasing atomic number of anions from sulfur to trillium. Also, increasing trend can be indicated in value of dielectric constant. All of this goes back to their electronic arrangement and photon interaction with electrons in different levels of energy.
- Optical absorption spectra are discussed in detail. The first region of the absorption spectrum for x direction is almost created by electron excitation from $3p_z$ orbital of sulfur atoms to $sp^2 - p$ antibonding orbitals. This transition occurs in that part of $sp^2 - p$ antibonding orbital which is of the space symmetry of s^* in Cd atom (s antibonding orbital). This knowledge and the value of photon energy for these transitions can lead to their applications in devices such as solar cells.

These results lead to the conclusion that these compounds can be efficiently used in optoelectronic devices working in the visible and UV range of the electromagnetic spectrum.

Acknowledgements

Computing resources used in this work were provided by the Nano-Fanavaran of Bistoon, High Performance and Grid Computing Center, Kermanshah, Iran.

Appendix A. Supplementary material

Supplementary material related to this article can be found online at http://dx.doi.org/10.1016/j.physleta.2016.11.040.

References

[1] E.A. Turner, H. Rösner, D. Fenske, Y. Huang, J.F. Corrigan, Characterization of ZnE (E = S, Se, or Te) materials synthesized using silylated chalcogen reagents in mesoporous MCM-41, J. Phys. Chem. B 110 (2006) 16261–16269.
[2] J. Gu, E. Fahrenkrug, S. Maldonado, Analysis of the electrodeposition and surface chemistry of CdTe, CdSe, and CdS thin films through substrate-overlayer surface-enhanced Raman spectroscopy, Langmuir 30 (2014) 10344–10353.
[3] R. Khenata, A. Bouhemadou, M. Sahnoun, A.H. Reshak, H. Baltache, M. Rabah, Elastic, electronic and optical properties of ZnS, ZnSe and ZnTe under pressure, Comput. Mater. Sci. 38 (2006) 29–38.
[4] Sh. Wei, J. Lu, Y. Qian, Density functional study of 2D semiconductor CdSe.hda$_{0.5}$ (hda = 1,6-hexanediamine) and its excitonic optical properties, Chem. Mater. 20 (2008) 7220–7227.
[5] R.A. Casali, N.E. Christensen, Elastic constants and deformation potentials of ZnS and ZnSe under pressure, Solid State Commun. 108 (1998) 793–798.
[6] J. Sörgel, U. Scherz, Ab initio calculation of elastic constants and electronic properties of ZnSe and ZnTe under uniaxial strain, Eur. Phys. J. B 5 (1998) 45–52.
[7] H.Y. Wang, J. Cao, X.Y. Huang, J.M. Huang, Pressure dependence of elastic and dynamical properties of zinc-blende ZnS and ZnSe from first principle calculation, Condens. Matter Phys. 15 (2012) 1–10, arXiv:1204.6102.
[8] M. Bilal, M. Shafiq, I. Ahmad, I. Khan, First principle studies of structural, elastic, electronic and optical properties of Zn-chalcogenides under pressure, J. Semicond. 35 (2014) 072001.
[9] W.U. Huynh, J.J. Dittmer, A.P. Alivisatos, Hybrid nanorod-polymer solar cells, Science 295 (2002) 2425–2427.
[10] X. Zong, G. Wu, H. Yan, G. Ma, J. Shi, F. Wen, L. Wang, C. Li, Photocatalytic H_2 evolution on MoS_2/CdS catalysts under visible light irradiation, J. Phys. Chem. C 114 (2010) 1963–1968.
[11] C. Soykan, S. Özdemir Kart, T. Cagin, Structural and mechanical properties of ZnTe in the zincblende phase, Arch. Mater. Sci. Eng. 46 (2010) 115–119.
[12] O. Zakharov, A. Rubio, X. Blase, M.L. Cohen, S.G. Louie, Quasiparticle band structures of six II–VI compounds: ZnS, ZnSe, ZnTe, CdS, CdSe, and CdTe, Phys. Rev. B 50 (1994) 10780–10787.
[13] T.E. Lister, J.L. Stickney, Formation of the first monolayer of CdSe on Au(111) by electrochemical ALE, Appl. Surf. Sci. 107 (1996) 153–160.
[14] S. Ithurria, B. Dubertret, Quasi 2D colloidal cdse platelets with thicknesses controlled at the atomic level, J. Am. Chem. Soc. 130 (2008) 16504–16505.

[15] T. Gao, T. Wang, Two-dimensional single crystal cds nanosheets: synthesis and properties, Cryst. Growth Des. 10 (2010) 4995–5000.
[16] M.A. Mahdi, J.J. Hassan, S.S. Ng, Z. Hassan, N.M. Ahmed, Synthesis and characterization of single-crystal CdS nanosheet for high-speed photodetection, Physica E 44 (2012) 1716–1721.
[17] H.H. Gürel, Hilmi Ünlü, Density functional and tight binding theories of electronic properties of II–VI heterostructures, Mater. Sci. Semicond. Process. 16 (2013) 1619–1628.
[18] J. Wang, J. Meng, Q. Li, J. Yang, Single-layer cadmium chalcogenides: promising visible-light driven photocatalysts for water splitting, Phys. Chem. Chem. Phys. 18 (2016) 17029–17036.
[19] W.-Z. Xiao, L.-L. Wang, J.-Y. Yang, First-principles calculations of electronic and magnetic properties in semi-fluorinated CdS sheet, Phys. Lett. A 376 (2012) 3401–3406.
[20] J.-P. Tang, W.-Z. Xiao, L.-L. Wang, X.-F. Li, Half-metallicity in carbon-substituted CdS monolayer, Physica E 59 (2014) 230–234.
[21] H. Zheng, et al., Monolayer II–VI semiconductors: a first-principles prediction, Phys. Rev. B 92 (2015) 115307.
[22] F. Tran, P. Blaha, Accurate band gaps of semiconductors and insulators with a semilocal exchange-correlation potential, Phys. Rev. Lett. 102 (2009) 226401.
[23] I. Khan, I. Ahmad, Theoretical studies of the band structure and optoelectronic properties of ZnO_xS_{1-x}, Int. J. Quant. Chem. 113 (2013) 1285–1292.
[24] I. Khan, I. Ahmad, H.A.R. Aliabad, M. Maqbool, Effect of phase transition on the optoelectronic properties of $Zn_{1-x}Mg_xS$, J. Appl. Phys. 112 (2012) 073104.
[25] I. Khan, A. Afaq, H.A.R. Aliabad, I. Ahmad, Transition from optically inactive to active Mg-chalcogenides: a first principle study, Comput. Mater. Sci. 61 (2012) 278–282.
[26] I. Khan, H.A.R. Aliabad, W. Ahmad, Z. Ali, I. Ahmad, First principle optoelectronic studies of visible light sensitive CZT, Superlattices Microstruct. 63 (2013) 91–99.
[27] I. Khan, F. Subhan, I. Ahmad, Z. Ali, Structural and optoelectronic properties of Mg substituted ZTe (Z = Zn, Cd and Hg), J. Phys. Chem. Solids 83 (2015) 75–84.
[28] P. Hohenberg, W. Kohn, Inhomogeneous electron gas, Phys. Rev. 136 (1964) 864–871.
[29] W. Kohn, L.J. Sham, Self-consistent equations including exchange and correlation effects, Phys. Rev. 140 (1965) 1133–1138.
[30] P. Blaha, K. Schwarz, G.K.H. Madsen, D. Kvasnicka, J. Luitz, K. Schwarz, An Augmented PlaneWave + Local Orbitals Program for Calculating Crystal Properties, revised edition, WIEN2k 13.1 (Release 06/26/2013), Wien2K Users Guide, ISBN 3-9501031-1-9501031-2.
[31] J.P. Perdew, K. Burke, M. Ernzerhof, Generalized gradient approximation made simple, Phys. Rev. Lett. 77 (1996) 3865–3868.
[32] H. Ehrenreich, M.H. Cohen, Self-consistent field approach to the many-electron problem, Phys. Rev. 115 (1959) 786–790.
[33] F. Birch, Equation of state and thermodynamic parameters of NaCl to 300 kbar in the high-temperature domain, J. Geophys. Res. B 83 (1978) 1257–1268.
[34] W.Z. Xiao, L.L. Wang, Magnetic properties in CdS monolayer doped with first-row elements: a density functional theory investigation, Phys. Status Solidi 251 (2014) 1257–1264.
[35] N. Chen, G. Yu, X. Gu, L. Chen, Y. Xie, F. Liu, F. Wang, X. Ye, W. Shi, Band structure engineering of CdSe nanosheet by strain: a first-principles study, Chem. Phys. Lett. 595–596 (2014) 91–96.
[36] Q. Peng, L. Han, X. Wen, Sh. Liu, Zh. Chen, J. Lian, S. De, Mechanical properties and stabilities of g-ZnS monolayers, RSC Adv. 5 (2015) 11240–11247.
[37] S. Kasap, P. Capper, Springer Handbook of Electronic and Photonic Materials, Springer, US, 2007.
[38] K.H. Hellwege, O. Madelung, Numerical Data and Functional Relationships in Science and Technology, Landolt-Börnstein, New Series, Group III, vols. 17a and 22a, Springer, New York, 1982.
[39] O. Madelung, Landolt-Börnstein: Numerical Data and Functional Relationships in Science and Technology, Springer, Berlin, 1984.
[40] A.K. Geim, K.S. Novoselov, The rise of graphene, Nat. Mater. 6 (2007) 183–191.
[41] D. Pacilé, J.C. Meyer, Ç.Ö. Girit, A. Zettl, The two-dimensional phase of boron nitride: few-atomic-layer sheets and suspended membranes, Appl. Phys. Lett. 92 (2008) 133107.
[42] T. Fujiwara, Y. Ishii, Quasicrystals, Elsevier, USA, 2008.
[43] R. Abt, C.A. Draxl, P. Knoll, Optical response of high temperature superconductors by full potential LAPW band structure calculations, Physica B 194–196 (1994) 1451–1452.
[44] M. Gajdoš, K. Hummer, G. Kresse, J. Furthmüller, F. Bechstedt, Linear optical properties in the projector-augmented wave methodology, Phys. Rev. B 73 (2006) 045112.
[45] C. Kittel, Introduction to Solid State Physics, Wiley Eastern Limited, New York, 1983.
[46] F. Wooten, Optical Properties of Solids, Academic Press, Inc., New York, London, 1972.
[47] M. Fox, Optical Properties of Solids, Oxford University Press, Oxford, 2010.